analytical chemistry

pubs.acs.org/ac

Article

Leucine Aminopeptidase-Mediated Multifunctional Molecular Imaging Tool for Diagnosis, Drug Evaluation, and Surgical Guidance of Liver-Related Diseases

Lanlan Xu, Mo Ma, Jingkang Li, Dejiang Gao, Pinyi Ma,* Fangmei Zhang,* and Daqian Song*

Cite This: *Anal. Chem.* 2023, 95, 12089−12096

Read Online

ACCESS | Metrics & More | Article Recommendations | Supporting Information

ABSTRACT: Traditional molecular imaging tools used for detecting liver diseases own several drawbacks, such as poor optical performance and limited applicability. Monitoring the concentration of leucine aminopeptidase (LAP), which is closely related to liver diseases such as liver cancer and liver injury, and analyzing it in diagnosis, drug evaluation, and surgical treatment is still a challenging task. Herein, we construct an intramolecular charge-transfer mechanism-based, ultrasensitive, near-infrared fluorescent probe (LAN-lap) for dynamic monitoring of LAP fluctuations in living systems. LAN-lap, with high specificity, stability, sensitivity, and water solubility, can achieve in vitro monitoring of LAP through both fluorescence and colorimetric methods. Moreover, LAN-lap can successfully be used for the localization imaging of endogenous LAP, confirming the upregulation of LAP expression in liver cancer and liver injury cells. In addition, LAN-lap can realize the imaging of liver tumors in living organisms. Meanwhile, it can intuitively present the degree of drug-induced liver injury, achieving semi-quantitative imaging evaluation of the hepatotoxicity of two drugs. Furthermore, LAN-lap can track liver cancer tumors in mice with peritoneal metastasis and can assist in fluorescence-guided surgical resection of liver cancer tumors. This multifunctional LAN-lap probe could play an important role in facilitating simultaneous diagnoses, imaging, and synergistic surgical navigation to achieve better point-of-care therapeutic efficacy.

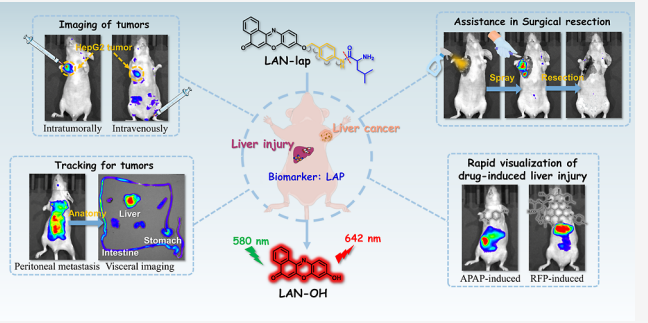

INTRODUCTION

Liver-related diseases pose a serious threat to human health, leading to nearly two million deaths worldwide every year.[1−3] Drug-induced liver injury (DILI), as the most common liver disease,[4,5] is the main reason leading to the cessation of clinical trials of new drugs and the withdrawal (about 30%) of drug candidates after marketing in recent years.[6,7] Therefore, utilizing specific biomarkers for timely and accurate evaluation of a drug's hepatotoxicity is of great significance for the development of new drugs and ensuring the safety of clinical medications. Additionally, as one of the most serious liver diseases, liver cancer is a malignant tumor that seriously endangers human health worldwide.[8−10] Accordingly, it is of great importance to develop a method for screening liver diseases as well as for evaluating the drug's hepatotoxicity.

Leucine aminopeptidase (LAP), a proteolytic enzyme that can specifically catalyze the hydrolysis of N-terminal leucine in proteins or peptides,[11−13] is widely found in microorganisms, plants, animals, and humans.[14,15] Previous studies have found that LAP is involved in various physiological and pathological processes and is closely related to cell proliferation, invasion, angiogenesis, and so forth.[16−19] LAP can be used not only as a biomarker for DILI diagnosis[20,21] but also as a cancer-related marker,[19,22,23] for instance, for liver cancer, ovarian epithelial malignant tumors, and breast cancer.[24−26]

In recent years, fluorescent probe technology has been widely applied in disease diagnosis and bioimaging due to its many advantages, including simple operation, non-destructive analysis, high spatial and temporal resolution, and imaging capacity.[27−29] So far, only a few studies have reported fluorescent probes using LAP as a medium for diagnosing liver disease. For example, Su et al.,[30] Zhang et al.,[31] and Wu et al.[21] have reported their application in diagnostic strategies for liver injury diseases, respectively, but the application of LAP in the diagnosis of liver cancer has not been discussed. Ma et al.[32] have conducted a preliminary exploration of imaging LAP in liver injury and liver cancer without performing in-depth studies. Besides, all these probes were constructed based on semi-cyanine structures, which have disadvantages such as

Received: May 16, 2023
Accepted: July 20, 2023
Published: July 31, 2023

Scheme 1. Synthetic Route of Probe LAN-Lap

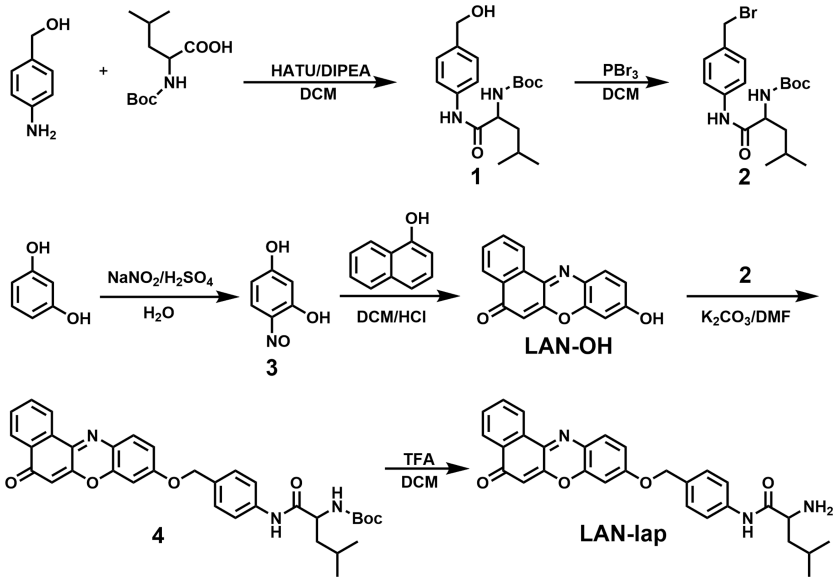

small Stokes shifts, low quantum yields, and poor water solubility. In view of this, it is still challenging to further develop a fluorescent probe with excellent performance and diverse application scenarios.

In our previous work, we designed a new fluorophore called LAN-OH,[27] which has several advantages, including a high fluorescence quantum yield (Φ = 0.47), a higher Stocks shift than the semi-cyanine structure, an emission peak covering the near-infrared region, good water solubility, and high stability. The exposed hydroxyl structure can combine with different recognition groups through esterification, etherification, and other reactions. However, LAN-OH used for designing and synthesizing the LAP-responsive probe cannot be directly completed due to the influence of the specific recognition site of L-leucine residue. In this work, we utilized *p*-aminobenzyl alcohol as a linker to connect the LAN-OH with L-leucine residue and successfully constructed an ultrasensitive near-infrared fluorescence probe LAN-lap (2-amino-4-methyl-*N*-(4-(((5-oxo-5*H*-benzo[*a*]phenoxazin-9-yl)oxy)methyl)phenyl)-pentanamide) for LAP detection. L-Leucine residue not only serves as the recognition group of LAP but also quenches the fluorescence of LAN-lap (Φ < 0.01), resulting in a low fluorescence background in detection. The *p*-aminobenzyl alcohol linker, on the one hand, converts the hydroxyl group to the amino group, expanding the application range of the fluorophore LAN-OH; on the other hand, compared with the direct link between the recognition group and fluorophore, the steric hindrance generated around the L-leucine residue group is reduced, thereby increasing the binding ability between LAN-lap and the recognition site on the target enzyme. After the systematic investigation of the spectral characteristics and analytical performance of LAN-lap, the ability of LAN-lap to image LAP in hepatocellular carcinoma and injured liver cells was studied. Encouraged by the excellent cell imaging performance, the ability of LAN-lap to image liver tumors and monitor liver injury in vivo was further investigated, and the drugs' hepatotoxicity of two drugs was evaluated. In addition, the ability of LAN-lap to track tumors in peritoneal metastasis models and guide surgical resection of liver tumors was also investigated. The results confirmed that LAN-lap could be used for the diagnosis of liver cancer and liver injury in vivo, the rapid assessment of the drug's hepatotoxicity, the tracking of liver tumors, and the navigation of liver tumor resection. Therefore, LAN-lap is a promising multifunctional molecular imaging diagnostic tool for clinical practical utilization.

EXPERIMENTAL PROCEDURE

Synthesis of LAN-Lap. The synthetic route of LAN-lap is shown in Scheme 1. Compounds **1**, **2**, **3**, and **LAN-OH** were synthesized according to previously reported methods.[33−35]

Synthesis of Compound 4. LAN-OH (0.263 g, 1 mmol), compound 2 (0.398 g, 1 mmol), and K_2CO_3 (0.138 g, 1 mmol) were successively dissolved in 10 mL of dimethylformamide and stirred for 3 h at room temperature. Then, saturated salt water was poured into the flask, and the generated precipitate was collected for further purification by silica gel column chromatography (CH_2Cl_2/CH_3OH = 30:1) to obtain compound 4 as a yellow solid, 78% yield.

Synthesis of the Probe LAN-Lap. Compound **4** (0.26 g, 0.446 mmol) was dissolved in 5 mL of CH_2Cl_2. Then, 1 mL of TFA was added dropwise into the flask and stirred for 1 h at room temperature. At last, saturated salt water was poured into the flask, and the organic layer was collected for further purification by silica gel column chromatography (CH_2Cl_2/CH_3OH = 20:1) to obtain the probe LAN-lap as a yellow solid, 81% yield. ^{1}H NMR (500 MHz, $CDCl_3$): δ 9.63 (s, 1H), 8.67 (d, *J* = 7.3 Hz, 1H), 8.28 (d, *J* = 7.1 Hz, 1H), 7.71 (ddd, *J* = 25.5, 15.9, 7.2 Hz, 6H), 7.41 (d, *J* = 7.9 Hz, 2H), 6.97 (d, *J* = 7.8 Hz, 1H), 6.86 (s, 1H), 6.41 (s, 1H), 5.11 (s, 2H), 3.58−3.46 (m, 1H), 1.86−1.76 (m, 2H), 1.49−1.41 (m, 1H), 0.98 (d, *J* = 7.0 Hz, 6H) (Figure S1). ^{13}C NMR (126 MHz, $CDCl_3$): δ 183.89, 173.83, 161.51, 151.36, 145.46, 144.37, 138.15, 132.02, 131.85, 131.52, 131.22, 131.03, 130.90, 128.44, 127.67, 125.85, 124.36, 119.54, 113.56, 106.98, 101.21, 70.50, 53.92, 43.86, 25.02, 23.45, 21.32 (Figure S2). MS (*m*/*z*) for $C_{29}H_{27}N_3O_4^+$ $[M + H]^+$ calcd, 482.2074; found: 482.2070 (Figure S3).

Detection of LAP in Solution. LAN-lap was dissolved in dimethyl sulfoxide (DMSO) to prepare a 1 mM stock solution.

https://doi.org/10.1021/acs.analchem.3c02130
Anal. Chem. 2023, 95, 12089−12096

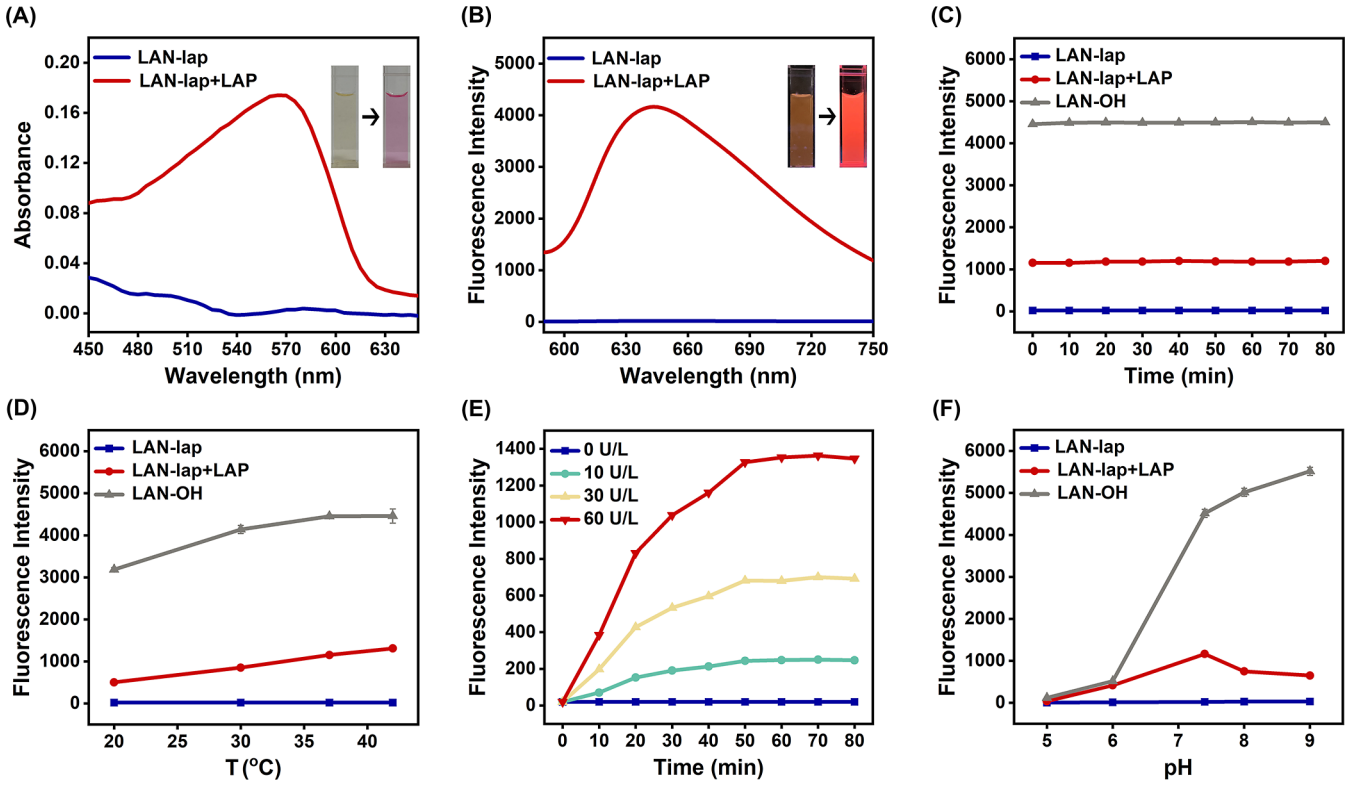

Figure 1. (A)/(B) Fluorescence/absorption spectra of LAN-lap (10 μM) and the reaction system (10 μM of LAN-lap and 400 U/L of LAP). (C) Photostability of LAN-lap (10 μM), LAN-OH (10 μM), and the reaction system (10 μM of LAN-lap and 400 U/L of LAP) continuously irradiated with 580 nm light for 80 min. (D) Thermal stability of LAN-lap (10 μM), LAN-OH (10 μM), and the reaction system (10 μM of LAN-lap and 50 U/L of LAP) at a temperature range of 25−42 °C. (E) Time-dependent fluorescence intensity of LAN-lap (10 μM) in the presence of LAP at various concentrations. (F) Effect of pH on LAN-lap (10 μM), LAN-OH (10 μM), and the reaction system (10 μM of LAN-lap and 50 U/L of LAP).

The test sample solution (1 mL) was prepared by mixing 10 μM LAN-lap, a certain concentration of analyte, and phosphate-buffered saline (PBS) (10 mM, pH 7.4) before subjecting it to measurements by a fluorescence spectrometer and a UV−vis spectrophotometer. Unless otherwise specified, the testing system was allowed to react at 37 °C in a PBS buffer solution (10 mM, pH 7.4) containing 1% (v/v) DMSO for 50 min before the test. In fluorescence measurements, the excitation wavelength was set at 580 nm, with a slit width of 2.5/2.5 nm and a PMT voltage of 700 V. The emission spectrum was recorded from 590 to 750 nm. In measurements using a UV−vis spectrophotometer, the absorption spectrum was recorded from 450 to 650 nm, and a 1 cm quartz cuvette was used.

RESULTS AND DISCUSSION

Characterization of LAN-Lap. The absorption and fluorescence spectra of LAN-lap were investigated. The absorption spectrum (Figure 1A) showed that the addition of LAP significantly enhanced the absorption peak at 575 nm of LAN-lap, accompanied by a visible color change of the solution from light yellow to red. The fluorescence spectrum of LAN-lap, as shown in Figure 1B, displayed that the addition of LAP significantly enhanced the emission peak at 642 nm of LAN-lap upon being excited by 580 nm light, accompanied by the change in color of the solution from yellow to bright red under the exposure to 365 nm light. The above results indicated that LAN-lap could effectively detect LAP by fluorescence and colorimetric methods.

The photostability of LAN-lap, LAN-OH, and the reaction system was further investigated. As shown in Figure 1C, the fluorescence intensity of LAN-lap, LAN-OH, and the reaction system remained roughly unchanged under continuous irradiation of 580 nm light for 80 min, indicating good photostability of them. The effects of temperature on LAN-lap, LAN-OH, and the reaction system were conducted. As shown in Figure 1D, the fluorescence intensity of LAN-lap at a temperature range of 25−42 °C was steady, while that of LAN-OH and the reaction system gradually increased with the increase in temperature. It was speculated that the increase of temperature within an appropriate range might accelerate the enzymatic reaction. The change in fluorescence intensity of the reaction system with time was analyzed (Figure 1E), and the results showed that the fluorescence intensity of the reaction system gradually increased with time and reached its maximum value at about 50 min. The effect of pH is shown in Figure 1F. Maximum enhancement of fluorescence intensity of the reaction system was observed at around pH 7.4, and it was deduced that LAP exhibits weaker activity in acidic and alkaline environments but presents higher activity at pH 7.4. Based on the above results and the physiological conditions, subsequent in vitro reactions were performed in PBS (10 mM, pH 7.4) at 37 °C for 50 min before detection.

Analytical Performance of LAN-Lap. The performance of LAN-lap in the quantitative detection of LAP using fluorescence and colorimetric methods was investigated under optimal experimental conditions. The results from quantitative detection by fluorescence method are illustrated in

https://doi.org/10.1021/acs.analchem.3c02130
Anal. Chem. 2023, 95, 12089−12096

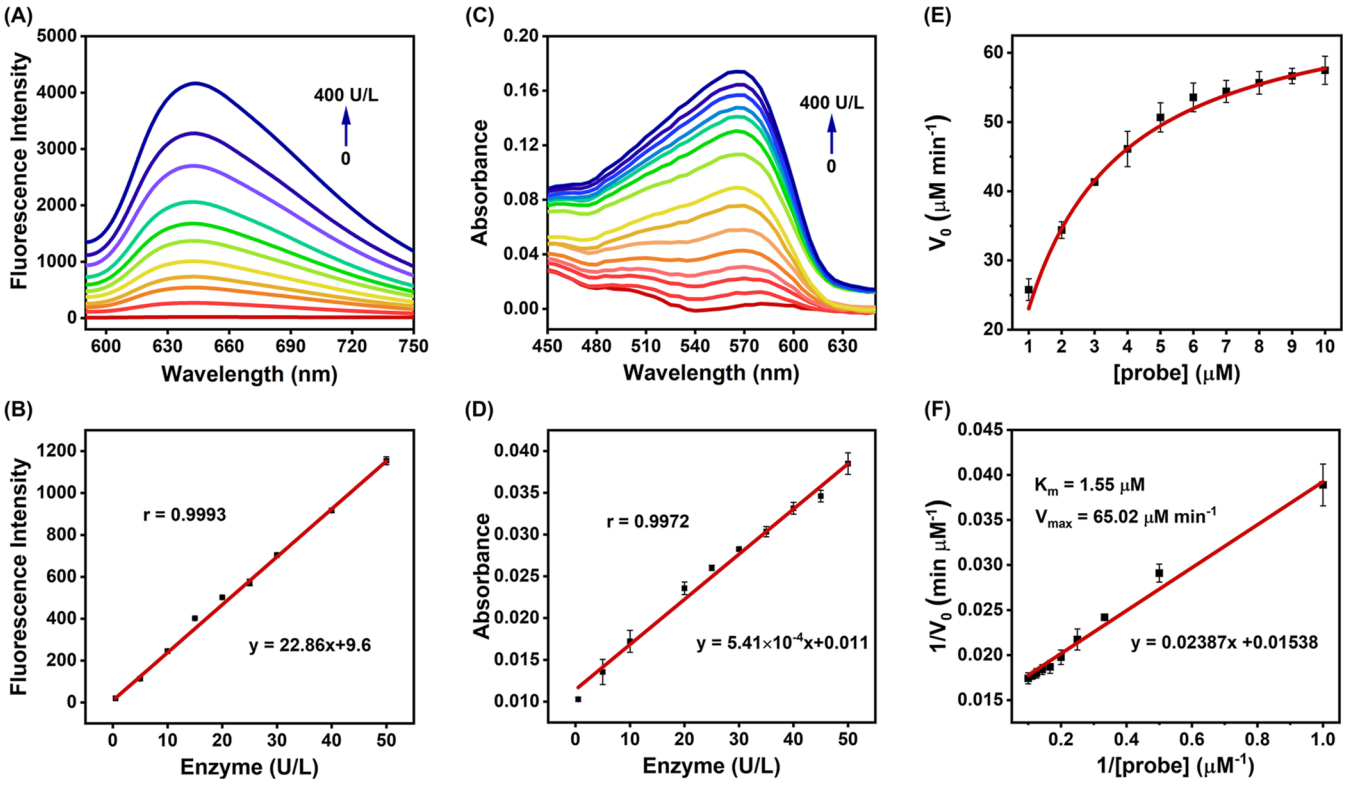

Figure 2. (A) Fluorescence spectra of LAN-lap (10 μM) in response to different concentrations of LAP. (B) Linear relationship between fluorescence intensity at 642 nm of the reaction system and LAP concentration (0.5−50 U/L). (C) Absorption spectra of LAN-lap (10 μM) in response to different concentrations of LAP. (D) Linear relationship between absorbance at 575 nm of the reaction system and LAP concentration (0.5−50 U/L). (E) Michaelis−Menten diagram for the enzymatic reaction between LAP (36 U/L) and LAN-lap at various concentrations (1, 2, 3, 4, 5, 6, 7, 8, 9, and 10 μM). (F) Lineweaver−Bulk plot for the enzymatic reaction.

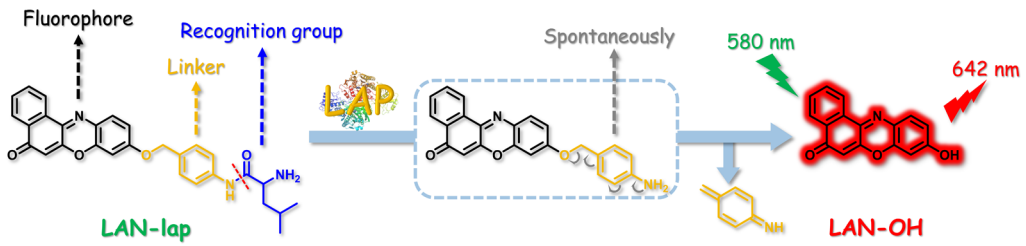

Figure 3. Sensing mechanism of LAN-lap toward LAP.

Figure 2A,B. The emission peak at 642 nm of the reaction system gradually increased with increasing LAP concentration upon excitation by 580 nm light. A good linear relationship (r = 0.9993) between the fluorescence intensity and LAP concentration (0.5−50 U/L) was observed, and the limit of detection (LOD) was as low as 0.0097 U/L. The fluorescence enhancement fold, excitation/emission wavelength, and LOD of LAN-lap were compared with those of other reported probes (Table S1). Apparently, the prepared LAN-lap owns even greater advantages. The results from quantitative detection using the colorimetric method are shown in Figure 2C,D. The absorption peak at 575 nm of the reaction system gradually increased with the increase of LAP concentration. The relationship between the absorbance and LAP concentration (0.5−50 U/L) was linear (r = 0.9972), and the LOD was 2.4 U/L. The above results indicate that LAN-lap can quantitatively detect LAP through both fluorescence and colorimetric methods.

Subsequently, the enzyme kinetics between LAN-lap and LAP was investigated. The Michaelis−Menten diagram and the Lineweaver−Burk plot are depicted in Figure 2E,F, and the maximum velocity (V_{max}) and the Michaelis constant (K_m) were calculated as 65.02 μM min^{-1} and 1.55 μM, which is far lower than that of L-leucine-4-p-nitroaniline (1.28 mM). The above results indicate that LAN-lap has good affinity and high sensitivity to LAP.

High selectivity is an important prerequisite allowing a probe to be able to accurately detect the analyte in complex systems. To evaluate the selectivity of LAN-lap to LAP, the effect of a series of potential interferences on LAN-lap was investigated. As revealed in Figure S4, interfering substances at a concentration of as high as 1 mM had no obvious impact on LAN-lap, unlike LAP. The above results are indicative of the high selectivity of LAN-lap to LAP.

Sensing Mechanism. The response mechanism of LAN-lap toward LAP was studied by mass spectrometry, high-performance liquid chromatography (HPLC) analysis, and

https://doi.org/10.1021/acs.analchem.3c02130
Anal. Chem. 2023, 95, 12089−12096

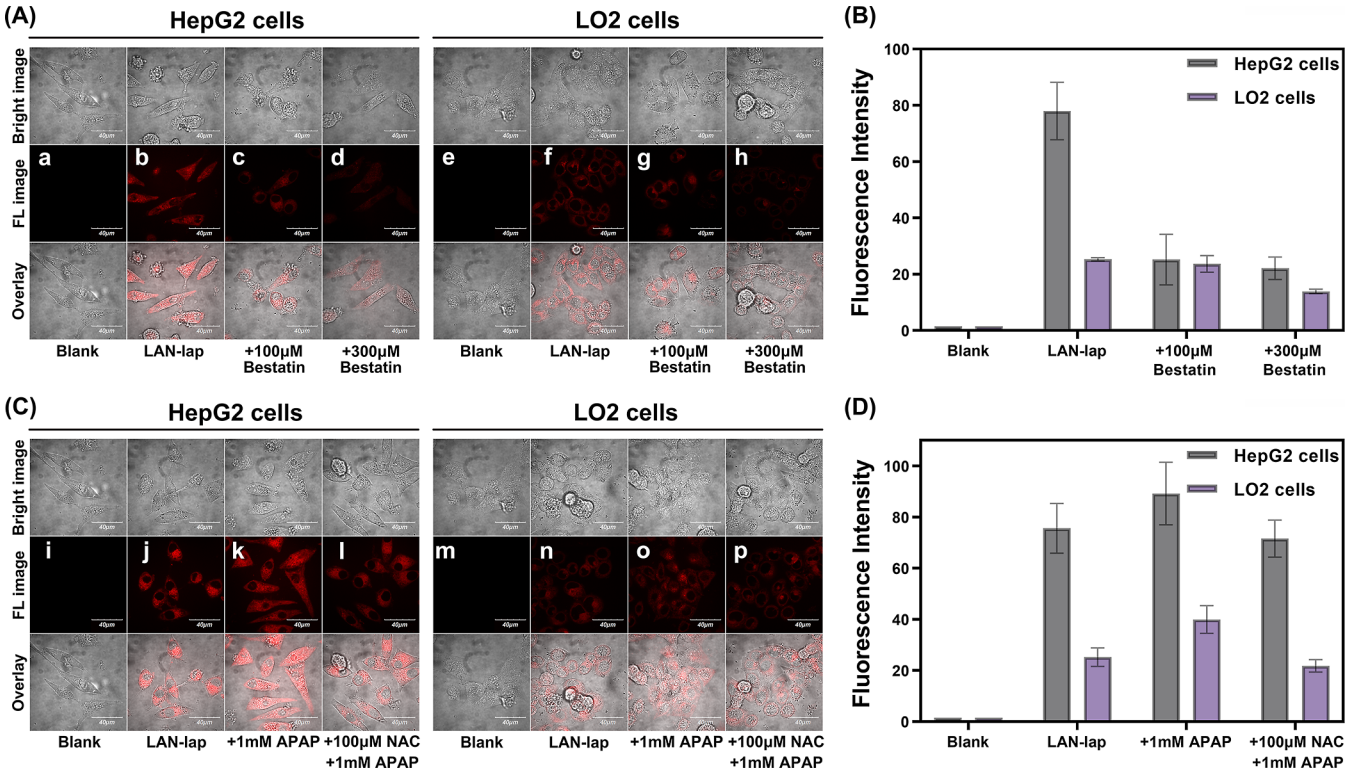

Figure 4. (A) Fluorescence images of endogenous LAP in HepG2 and LO2 cells. (B) Average fluorescence intensity of cells in (A). (C) Fluctuation of intracellular LAP levels in injured liver cells. (D) Average fluorescence intensity of cells in (C).

inhibitor experiments. The mass spectrometric results manifested that a mass peak of the reaction system appeared at m/z 264.0665 (Figure S5), which was consistent with the mass peak of LAN-OH (m/z 264.0659) (Figure S6). The HPLC analysis (Figure S7) illustrated the characteristic peaks of LAN-lap at 2.41 min and LAN-OH at 2.72 min, while the reaction system exhibited characteristic peaks at 2.41 and 2.72 min, which coincided with the peaks of LAN-lap and LAN-OH, respectively. The results from the inhibitor experiment are exhibited in Figure S8. The inhibitor bestatin had no inhibitory effect on the fluorescence intensity of LAN-lap and LAN-OH but significantly inhibited the fluorescence intensity of the reaction system. According to the results above, we believed the sensing mechanism of LAN-lap toward LAP (Figure 3) could be that LAP specifically recognizes and cut off the L-leucine residue on LAN-lap, leading to the spontaneous departure of the *p*-aminobenzyl alcohol linker, in turn resulting in the release of LAN-OH, and the detection of LAP is thereby realized.

A molecular docking simulation between LAN-lap and LAP was carried out. As shown in Figure S9A, LAN-lap forms 13 hydrogen bonds with 6 amino acids (Asn384, Phe387, Asn81, Trp383, Arg399, and Trp398) in LAP with a binding energy of as low as −10.1 kcal/mol, which is the indication that LAN-lap has a strong binding affinity to LAP. Theoretical calculations for the molecular orbitals of LAN-lap and LAN-OH were conducted (Figure S9B), and the results suggested that the response between LAN-lap and LAP was through the intramolecular charge transfer. The above results support the sensing mechanism proposed in Figure 3.

Imaging of LAP in Cells. Low cytotoxicity is a prerequisite for allowing the probe to be applied to cell imaging. Therefore, the cytotoxicity of LAN-lap to HepG2 cells was evaluated by CCK-8 analysis before cell imaging. As shown in Figure S10, in the presence of LAN-lap at a concentration of as high as 50 μM, the cells still had a survival rate of higher than 90%, which indicates that LAN-lap has low cytotoxicity.

Based on its low cytotoxicity, LAN-lap was further applied in cell imaging. First, the trend of intracellular fluorescence intensity with time was investigated. As shown in Figure S11, intracellular fluorescence intensity gradually increased with time; specifically, the increase was rapid during the first 1 h but slowed down in the subsequent 1 h. Therefore, 1 h was selected as the optimal time for incubating cells with LAN-lap in the following imaging experiments.

Second, the ability of LAN-lap to image endogenous LAP in liver cancer cells was investigated. As displayed in Figure 4A, compared with the control group (a,e), both HepG2 (b) and LO2 (f) cells generated fluorescence signals. However, the fluorescence signals in HepG2 cells were significantly stronger than those in LO2 cells, as can be more intuitively seen in Figure 4B. The addition of the inhibitor bestatin inhibited the fluorescence signals in both HepG2 and LO2 cells (c and d, and g and h), which further confirmed that the fluorescence signals observed in the cells were due to the response of LAN-lap to LAP. The above results confirm that the level of LAP was upregulated in liver cancer cells, and LAN-lap could be used for fluorescence imaging of intracellular LAP.

Third, the ability of LAN-lap to monitor the level of LAP in injured liver cells was investigated. As shown in Figure 4C, compared to HepG2 and LO2 cells (j and n), the cells in the liver injury group, which were pretreated with acetaminophen (APAP), showed stronger fluorescence signals (k and o). While cells in the groups (l and p) pretreated with NAC (*N*-acetylcysteine) and then with APAP showed a weaker fluorescence signal compared to those in the liver injury

https://doi.org/10.1021/acs.analchem.3c02130
Anal. Chem. 2023, 95, 12089−12096

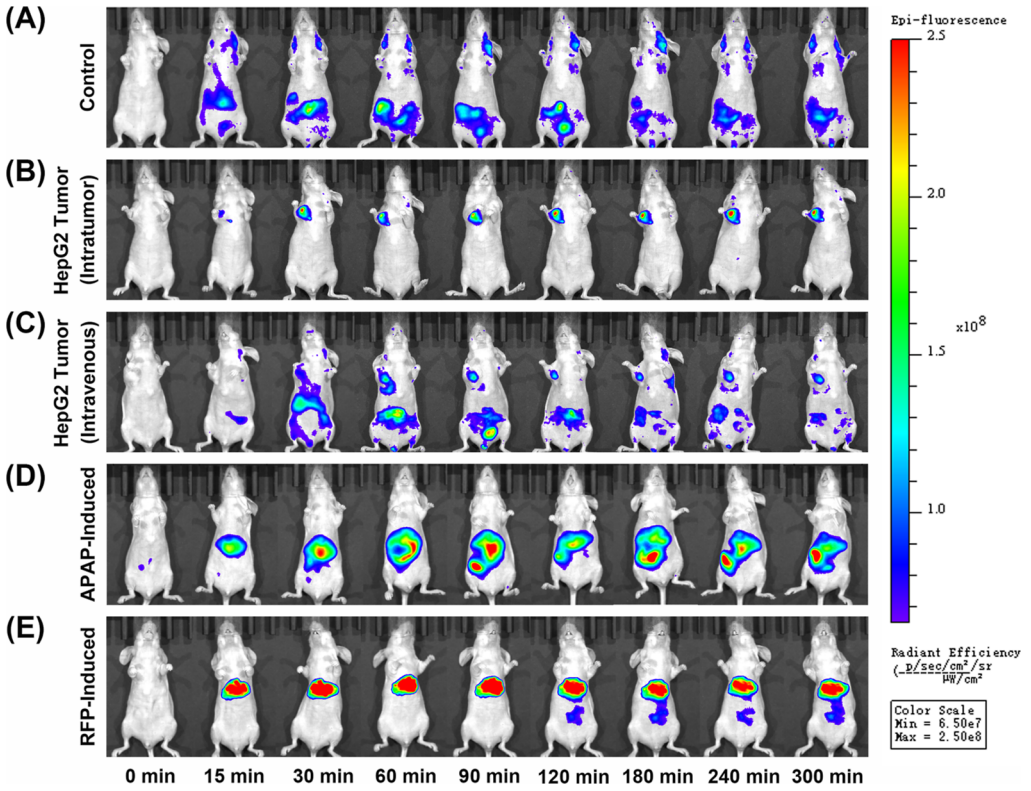

Figure 5. Fluorescence images of mice in the control group (A), intratumoral injection-tumor group (B), intravenous injection-tumor group (C), APAP-induced liver injury group (D), and RFP-induced cholestatic liver injury group (E) captured at 0−300 min after injection with LAN-lap.

group (k and o), as can be intuitively seen in Figure 4D. It can be deduced that the increase in LAP levels may be related to the deficiency of biothiols. The above results indicate that LAP levels in injured liver cells were upregulated, and LAN-lap could be used to monitor the fluctuation of LAP levels in injured liver cells.

Imaging of LAP *In Vivo*. Encouraged by its excellent ability in cell imaging, LAN-lap was further employed to image LAP in vivo. First, the mice were divided into five groups: control group, intratumoral injection-tumor group, intravenous injection-tumor group, APAP-induced liver injury group, and RFP-induced cholestatic liver injury group (RFP, Rifampicin, an antibiotic drug). The fluorescence images of the five groups of mice after injection with LAN-lap are shown in Figure 5. In the control group, it was observed that the mouse exhibited concentrated fluorescence signals in the abdomen during 0−120 min and then gradually weakened as time passed (Figure 5A). In the intratumoral injection-tumor group, the fluorescence signal was clearly observed at the site of the tumor until 30 min (Figure 5B). In the intravenous injection-tumor group, it was observed that fluorescence signals were concentrated in the abdomen before 120 min, then gradually weakened as time passed. Meanwhile, obvious fluorescence signals appeared at the tumor site as early as 60 min and gradually became clearer as time passed (Figure 5C). The above results indicate that the LAP level is upregulated in HepG2 tumors, and LAN-lap could visualize HepG2 tumors in vivo. In the APAP-induced liver injury group, strong fluorescence signals were observed at the site of the liver as early as 15 min, then gradually became stronger at both the liver and the abdomen (Figure 5D). In the RFP-induced cholestatic liver injury group (Figure 5E), it was observed that fluorescence signals were significantly stronger than those in the APAP-induced liver injury group as early as 15 min and roughly remained unchanged as time passed. The above results indicate that the LAP expression level is significantly upregulated in liver injury. Additionally, the degree of liver injury in RFP-induced cholestatic liver injury is more severer than that in APAP-induced liver injury, indicating that RFP has lower safety than APAP. Based on the above results, it is safe to draw a conclusion that LAN-lap could be used as a powerful tool to monitor LAP levels in vivo, visualize and diagnose liver cancer and injury, and quickly evaluate the drug's safety.

Confirming the ability to image LAP in HepG2 tumors in vivo, LAN-lap was further applied to track HepG2 tumors in peritoneal metastasis mice. As shown in Figure 6, compared with the mice in the control group (Figure 6A), mice bearing HepG2 tumors peritoneal metastasis (Figure 6B) exhibited stronger fluorescence signals in the liver and abdomen, suggesting that HepG2 tumors had metastasized to the liver and abdomen. Then, the mice in the two groups were dissected to take the main internal organs, including the heart, liver, spleen, lung, kidney, intestine, and stomach, then for fluorescence imaging. It was observed that the fluorescence signals of the viscera from peritoneal metastasis mice (Figure 6D) were stronger than those of the mice in the control group in general (Figure 6C), among which the fluorescence signals of the intestine, stomach, and particularly the liver were significantly higher, suggesting that HepG2 tumors metastasized mainly to the liver as well as the intestines and stomach. The results from visceral imaging confirmed our speculation that HepG2 tumors metastasized to the liver and abdomen. All the above results indicate that LAN-lap can be used for tracking tumors in a peritoneal metastasis model in vivo.

Finally, the ability of LAN-lap in fluorescence-guided surgical resection of tumors was investigated. As shown in

https://doi.org/10.1021/acs.analchem.3c02130
Anal. Chem. 2023, 95, 12089−12096

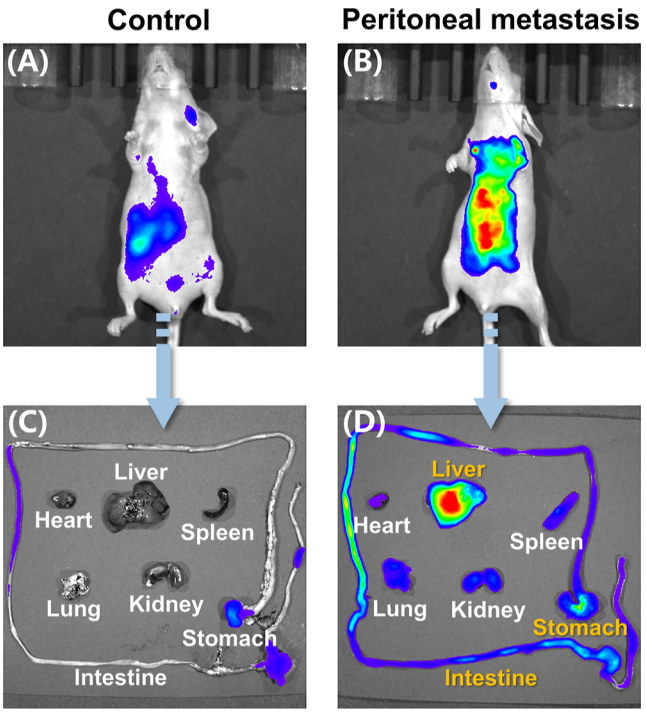

Figure 6. Fluorescence images of mice in the control group (A) and peritoneal metastasis group (B) captured at 1 h after intravenous injection with LAN-lap (200 μM, 100 μL). Fluorescence images of the viscera of mice in the control group (C) and peritoneal metastasis group (D).

Figure 7, the skin-peeled tumor site showed obvious fluorescent signals after being evenly sprayed with LAN-lap (Figure 7C). To avoid the irreversible damage to living organisms caused by excessive resection of normal tissue, the strategy of multiple conservative resection−imaging−resection was adopted during the surgical resection of tumors. At last, the skin-peeled area was sprayed with LAN-lap again to check for any remaining microscopic tumors until no fluorescence signals were exhibited, which was the indication that the tumor was completely removed (Figure 7D). The above results verified that the probe LAN-lap can be used in fluorescence-guided surgical resection of tumors.

CONCLUSIONS

In this work, we designed and synthesized an ultrasensitive fluorescence probe LAN-lap, which possesses high selectivity, stability, sensitivity, and water solubility and can quantitatively detect LAP through both fluorescence and colorimetric methods. Not only can the LAN-lap visualize endogenous LAP and confirm the upregulation of LAP level in liver cancer cells and injured liver cells but also it can visualize the level of LAP in vivo and confirm the significant upregulation of LAP level in HepG2 tumors, APAP-induced liver injury, and RFP-induced cholestasis liver injury. Besides, LAN-lap can be used for rapid evaluation of a drug's hepatotoxicity. In addition, LAN-lap was demonstrated to possess the ability to track tumors in a peritoneal metastasis model in vivo and assist in fluorescence-guided surgical resection of liver cancer tumors. Overall, LAN-lap is a promising multifunctional molecular imaging tool that can be used for the diagnosis of liver injury and liver cancer, as well as for the rapid assessment of the drug's hepatotoxicity and navigation in surgical resection of liver cancer.

ASSOCIATED CONTENT

Supporting Information

The Supporting Information is available free of charge at https://pubs.acs.org/doi/10.1021/acs.analchem.3c02130.

Additional experimental details, instruments and materials, synthesis, determination of the detection limit, determination of fluorescence quantum yield, enzymatic kinetics assays, molecular docking, theoretical calculation and analysis, cell culture, CCK-8 assay, imaging in cells, establishment of tumor model, imaging in vivo, ^{1}H-NMR spectrum of probe LAN-lap in $CDCl_3$, ^{13}C-NMR spectrum, mass spectrum, fluorescence intensity of LAN-lap, HPLC analysis, effect of the bestatin inhibitor on fluorescence intensity, molecular docking simulation, cytotoxicity assays of probe LAN-lap, trend of fluorescence intensity in HepG2 cells, and comparison of LAN-lap with the probes (PDF)

AUTHOR INFORMATION

Corresponding Authors

Pinyi Ma − *College of Chemistry, Jilin Province Research Center for Engineering and Technology of Spectral Analytical Instruments, Jilin University, Changchun 130012, China;* orcid.org/0000-0002-3230-4928; Email: mapinyi@jlu.edu.cn

Fangmei Zhang − *XNA Platform, Institute of Pharmaceutical Sciences, Zhengzhou University, Zhengzhou 450001, China;* Email: zhangfm701@zzu.edu.cn, muxin701@163.com

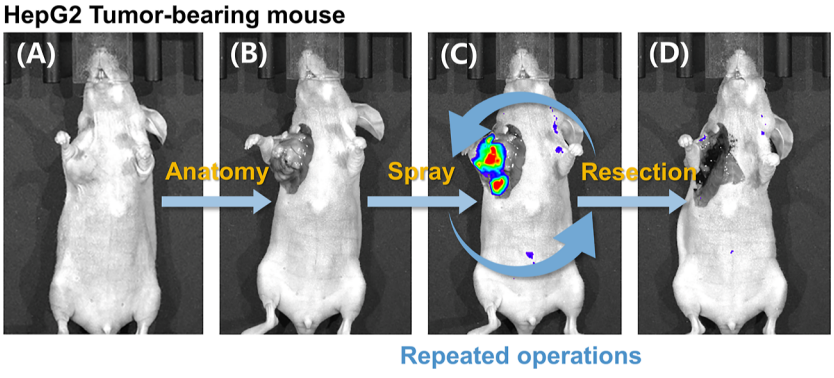

Figure 7. Procedure for tumor resection and fluorescence imaging.

https://doi.org/10.1021/acs.analchem.3c02130
Anal. Chem. 2023, 95, 12089−12096

Daqian Song − *College of Chemistry, Jilin Province Research Center for Engineering and Technology of Spectral Analytical Instruments, Jilin University, Changchun 130012, China;* orcid.org/0000-0002-4866-1292; Email: songdq@jlu.edu.cn

Authors

Lanlan Xu − *College of Chemistry, Jilin Province Research Center for Engineering and Technology of Spectral Analytical Instruments, Jilin University, Changchun 130012, China*

Mo Ma − *College of Chemistry, Jilin Province Research Center for Engineering and Technology of Spectral Analytical Instruments and School of Pharmacy, Jilin University, Changchun 130012, China*

Jingkang Li − *College of Chemistry, Jilin Province Research Center for Engineering and Technology of Spectral Analytical Instruments, Jilin University, Changchun 130012, China*

Dejiang Gao − *College of Chemistry, Jilin Province Research Center for Engineering and Technology of Spectral Analytical Instruments, Jilin University, Changchun 130012, China*

Complete contact information is available at: https://pubs.acs.org/10.1021/acs.analchem.3c02130

Notes

The authors declare no competing financial interest.

■ ACKNOWLEDGMENTS

This work was supported by the National Natural Science Foundation of China (22004046 and 22074052), the Science and Technology Developing Foundation of Jilin Province of China (nos. 20230204116YY, 20230505010 ZP, and YDZJ202302CXJD031), and the Special Scientific Research Starting Foundation for Young Teachers of Zhengzhou University (32213226).

■ REFERENCES

(1) Subudhi, P. D.; Bihari, C.; Sarin, S. K.; Baweja, S. *Nanotheranostics* **2022**, *6*, 365−375.
(2) de Gregorio, E.; Colell, A.; Morales, A.; Mari, M. *Int. J. Mol. Sci.* **2020**, *21*, 3858.
(3) Xu, D.; Tian, Y.; Xia, Q.; Ke, B. *Front. Immunol.* **2021**, *12*, 682736.
(4) Gijbels, E.; Devisscher, L.; Vinken, M. *Food Chem. Toxicol.* **2021**, *152*, 112165.
(5) Vilas-Boas, V.; Gijbels, E.; Leroy, K.; Pieters, A.; Baze, A.; Parmentier, C.; Vinken, M. *Int. J. Mol. Sci.* **2021**, *22*, 11005.
(6) Atallah, E.; Wijayasiri, P.; Cianci, N.; Abdullah, K.; Mukherjee, A.; Aithal, G. P. *BMC Gastroenterol.* **2021**, *21*, 244.
(7) Luo, G.; Shen, Y.; Yang, L.; Lu, A.; Xiang, Z. *Arch. Toxicol.* **2017**, *91*, 3039−3049.
(8) Cai, S.; Bi, Z.; Bai, Y.; Zhang, H.; Zhai, D.; Xiao, C.; Tang, Y.; Yang, L.; Zhang, X.; Li, K.; Yang, R.; Liu, Y.; Chen, S.; Sun, T.; Liu, H.; Yang, C. *Front. Oncol.* **2020**, *9*, 1431.
(9) Li, C.; Yang, J.; Liu, C.; Wang, X.; Zhang, L. *Pharmacol. Res.* **2020**, *158*, 104848.
(10) Zhang, D.; Pan, Y.; Yang, Z.; Zeng, H.; Wang, X.; Chen, J.; Wang, J.; Zhang, Y.; Zhou, Z.; Chen, M.; Hu, D. *J. Clin. Med.* **2022**, *12*, 324.
(11) Chen, Y. *Mater. Today Chem.* **2020**, *15*, 100216.
(12) Drinkwater, N.; Malcolm, T. R.; McGowan, S. *Biochimie* **2019**, *166*, 38−51.
(13) Sakabe, M.; Asanuma, D.; Kamiya, M.; Iwatate, R. J.; Hanaoka, K.; Terai, T.; Nagano, T.; Urano, Y. *J. Am. Chem. Soc.* **2013**, *135*, 409−414.
(14) Kondo, C.; Shibata, K.; Terauchi, M.; Kajiyama, H.; Ino, K.; Nomura, S.; Nawa, A.; Mizutani, S.; Kikkawa, F. *Int. J. Cancer* **2006**, *118*, 1390−1394.
(15) Zhou, Z.; Wang, F.; Yang, G.; Lu, C.; Nie, J.; Chen, Z.; Ren, J.; Sun, Q.; Zhao, C.; Zhu, W. H. *Anal. Chem.* **2017**, *89*, 11576−11582.
(16) Harbut, M. B.; Velmourougane, G.; Dalal, S.; Reiss, G.; Whisstock, J. C.; Onder, O.; Brisson, D.; McGowan, S.; Klemba, M.; Greenbaum, D. C. *Proc. Natl. Acad. Sci. U.S.A.* **2011**, *108*, E526−E534.
(17) Mei, J.; Kim, D. H.; Ayzner, A. L.; Toney, M. F.; Bao, Z. *J. Am. Chem. Soc.* **2011**, *133*, 20130−20133.
(18) Tsujimoto, M.; Goto, Y.; Maruyama, M.; Hattori, A. *Heart Fail. Rev.* **2008**, *13*, 285−291.
(19) Zhang, H.; Fan, J.; Wang, K.; Li, J.; Wang, C.; Nie, Y.; Jiang, T.; Mu, H.; Peng, X.; Jiang, K. *Anal. Chem.* **2014**, *86*, 9131−9138.
(20) Hou, X.; Yu, Q.; Zeng, F.; Yu, C.; Wu, S. *Chem. Commun.* **2014**, *50*, 3417−3420.
(21) Huang, Y.; Qi, Y.; Zhan, C.; Zeng, F.; Wu, S. *Anal. Chem.* **2019**, *91*, 8085−8092.
(22) Lee, M. H.; Kim, J. S.; Sessler, J. L. *Chem. Soc. Rev.* **2015**, *44*, 4185−4191.
(23) Van de Bittner, G. C.; Bertozzi, C. R.; Chang, C. J. *J. Am. Chem. Soc.* **2013**, *135*, 1783−1795.
(24) Wang, D.; Chen, J.; Ren, L.; Li, Q.; Li, D.; Yu, J. *Inorg. Chem. Front.* **2017**, *4*, 468−472.
(25) Wang, M. D.; Wang, Y.; Xia, Y. P.; Dai, J. W.; Gao, L.; Wang, S. Q.; Wang, H. J.; Mao, L.; Li, M.; Yu, S. M.; Tu, Y.; He, Q. W.; Zhang, G. P.; Wang, L.; Xu, G. Z.; Xu, H. B.; Zhu, L. Q.; Hu, B. *Mol. Neurobiol.* **2016**, *53*, 1310−1321.
(26) Yin, J.; Kwon, Y.; Kim, D.; Lee, D.; Kim, G.; Hu, Y.; Ryu, J. H.; Yoon, J. *J. Am. Chem. Soc.* **2014**, *136*, 5351−5358.
(27) Xu, L.; Chu, H.; Gao, D.; Wu, Q.; Sun, Y.; Wang, Z.; Ma, P.; Song, D. *Anal. Chem.* **2023**, *95*, 2949−2957.
(28) Yang, Y.; Zhang, L.; Wang, J.; Cao, Y.; Li, S.; Qin, W.; Liu, Y. *Anal. Chem.* **2022**, *94*, 13498−13506.
(29) Zhang, P.; Fu, C.; Liu, H.; Guo, X.; Zhang, Q.; Gao, J.; Chen, W.; Yuan, W.; Ding, C. *Anal. Chem.* **2021**, *93*, 11337−11345.
(30) Zhang, Y.; Chen, X.; Yuan, Q.; Bian, Y.; Li, M.; Wang, Y.; Gao, X.; Su, D. *Chem. Sci.* **2021**, *12*, 14855−14862.
(31) Cheng, D.; Peng, J.; Lv, Y.; Su, D.; Liu, D.; Chen, M.; Yuan, L.; Zhang, X. *J. Am. Chem. Soc.* **2019**, *141*, 6352−6361.
(32) He, X.; Li, L.; Fang, Y.; Shi, W.; Li, X.; Ma, H. *Chem. Sci.* **2017**, *8*, 3479−3483.
(33) Huang, X.; Lei, Q.; Huang, S.; Zeng, H.; Feng, B.; Zeng, Q.; Hu, Y.; Zeng, W. *Chem. Commun.* **2021**, *57*, 6608−6611.
(34) Xu, L.; Wu, M.; Zhao, L.; Han, H.; Zhang, S.; Ma, P.; Sun, Y.; Wang, X.; Song, D. *Talanta* **2020**, *215*, 120892.
(35) Xu, L.; Zhang, Y.; Zhao, L.; Han, H.; Zhang, S.; Huang, Y.; Wang, X.; Song, D.; Ma, P.; Ren, P.; Sun, Y. *Talanta* **2021**, *233*, 122578.